Electronic Supplementary Material (ESI) for Nanoscale.

Supporting Information

Table of contents:

1. The band structures of Bi_2Te_3 films with thicknesses *d* = 4~6 QLs.

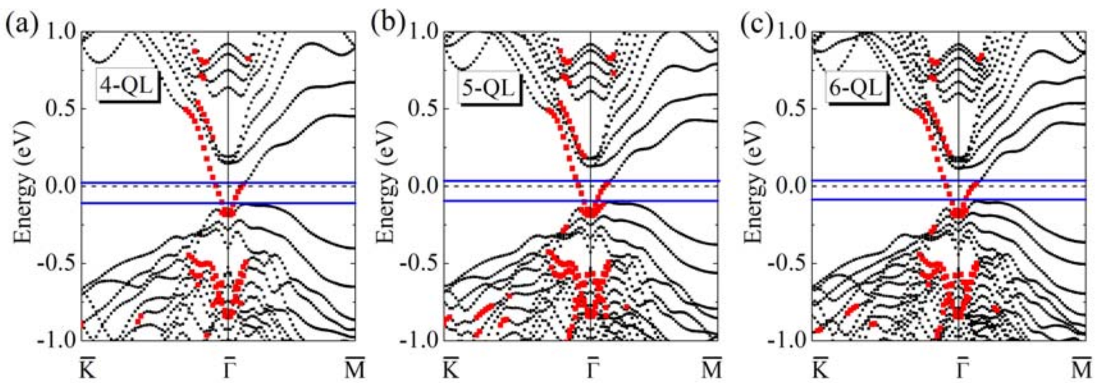

Figure S1 Band structures of Bi_2Te_3 films with thicknesses *d* = 4~6 QLs. The Fermi level is set to 0 eV. The blue lines indicate their bulk gaps. The identified surface states are marked by the red squares. For the 4-, 5-, and 6-QL films, the critical percentages of the projections onto the top-most or the bottom-most *quintuple layer* are 50%, 40%, 40%, respectively.

2. The transport coefficients and *ZT* value of Bi_2Te_3 film with thicknesses *d* = 3 QLs, plotted as a function of the carrier concentration. Due to the presence of topologically protected surface states and their delicate competition with the bulk states, it is quite different from those shown in Figure 2 with only trivial surface states (*d* = 1~2 QLs).

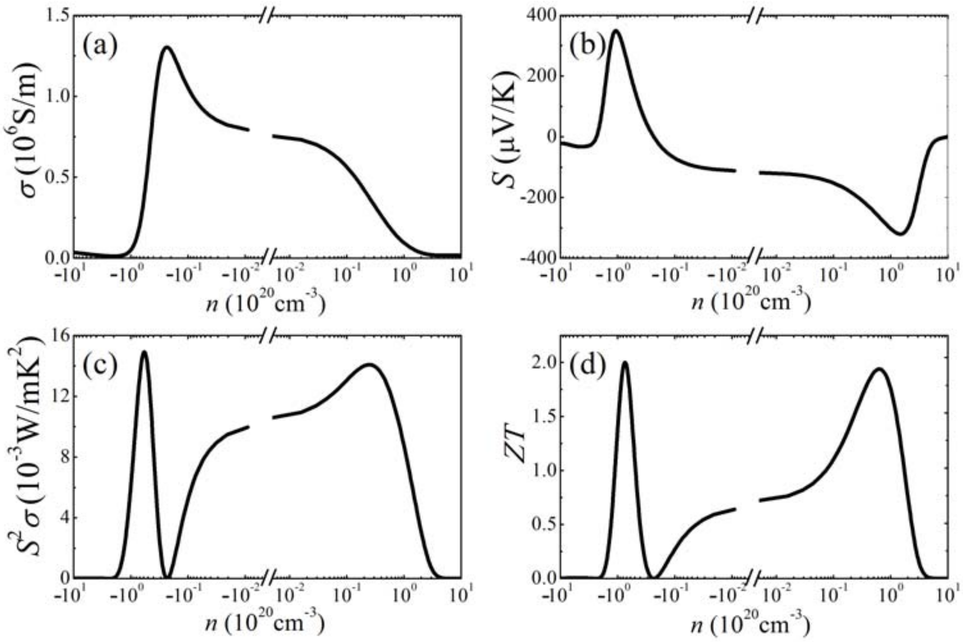

Figure S2 Calculated (a) electrical conductivity σ, (b) Seebeck coefficient S, (c) power factor $S^2\sigma$, and (d) figure of merit *ZT* as a function of the carrier concentration n for Bi_2Te_3 films with thicknesses *d* = 3 QLs. Positive and negative carrier concentrations represent *p*- and *n*-type carriers, respectively.

3. The following figures (Figure S3-S6) plot the TDF of Bi_2Te_3 films with thicknesses *d* = 3~6 QLs, where the relaxation time ratio is set as 1000 (corresponding to the highest *ZT* values in Figure 4).

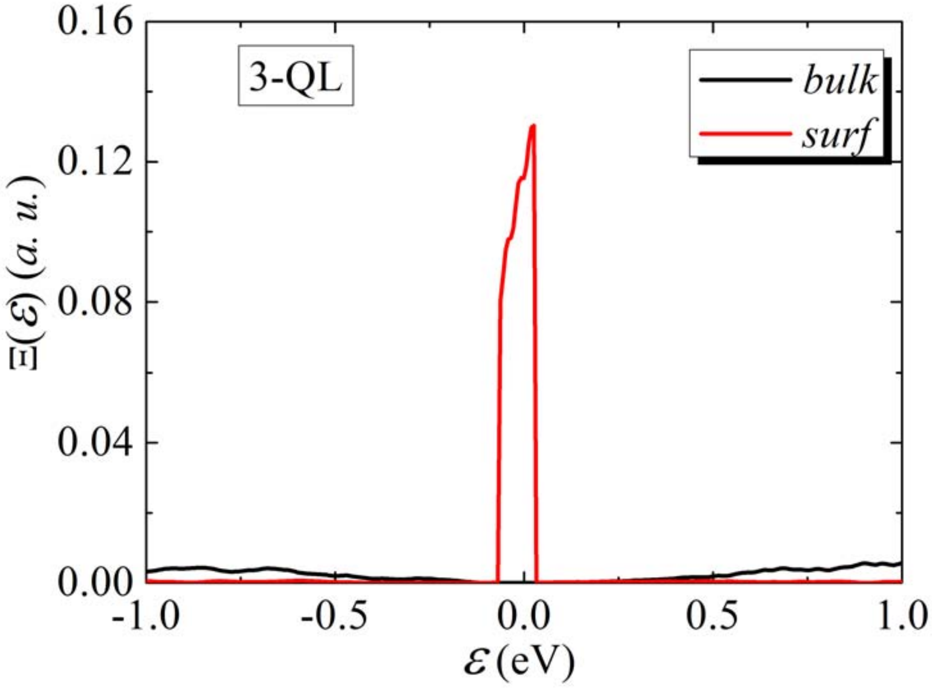

Figure S3 The bulk and surface TDF of 3-QL film.

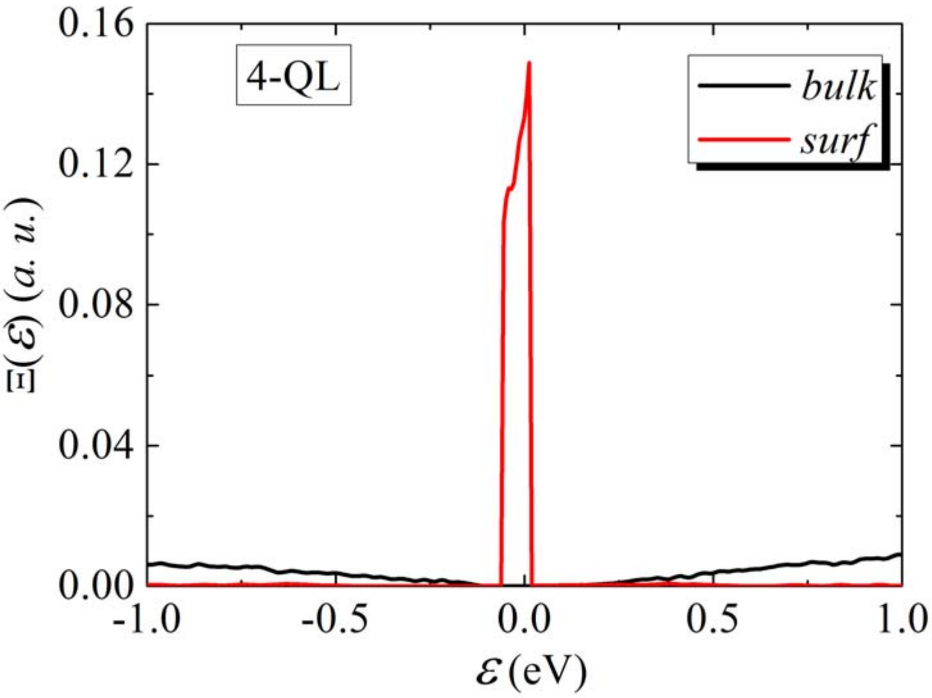

Figure S4 The bulk and surface TDF of 4-QL film.

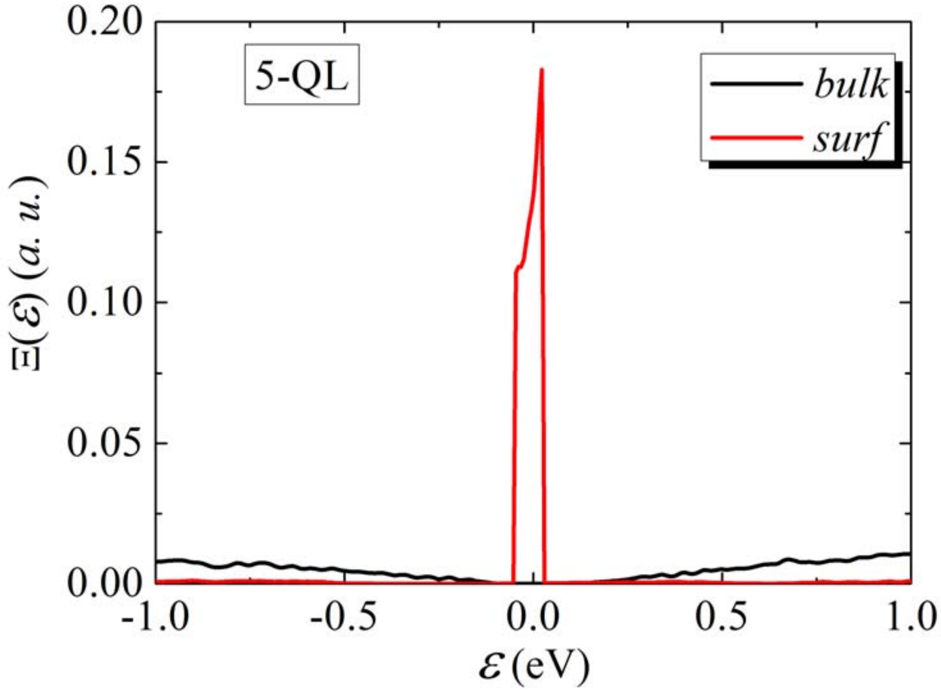

Figure S5 The bulk and surface TDF of 5-QL film.

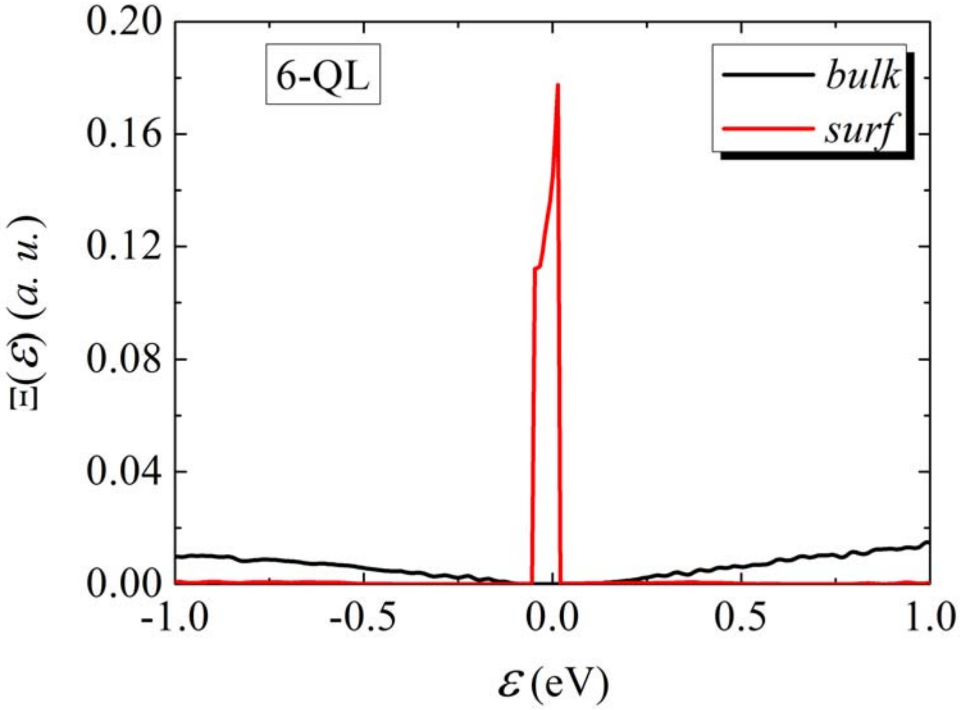

Figure S6 The bulk and surface TDF of 6-QL film.

4. Transport coefficients of *n*-type 3-QL Bi_2Te_3 film (Figure S7), and those with larger thicknesses *d* = 4~6 QLs (Figure S8-S13), plotted as a function of the relaxation time ratio.

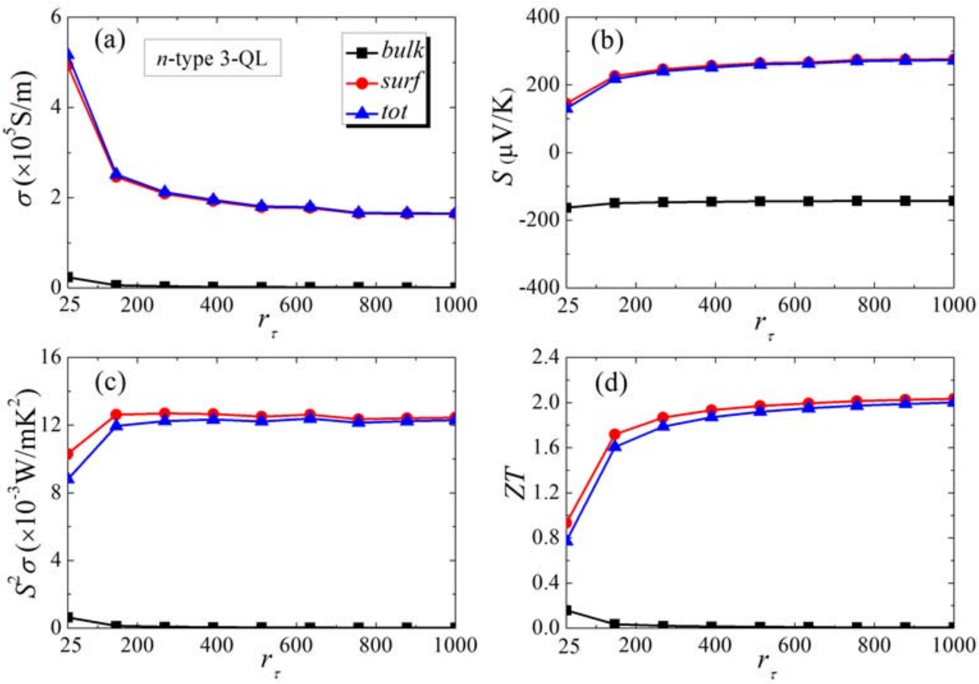

Figure S7 Calculated (a) electrical conductivity σ, (b) Seebeck coefficient S, (c) power factor $S^2\sigma$, and (d) figure of merit *ZT* of *n*-type 3-QL Bi_2Te_3 film as a function of the relaxation time ratio r_τ.

As shown in the following figures (Figures S8-S13), the variations of the transport coefficients of Bi_2Te_3 films with thicknesses d = 4~6 QLs exhibit similar r_τ dependence as for the 3-QL Bi_2Te_3 film shown in Figure 3.

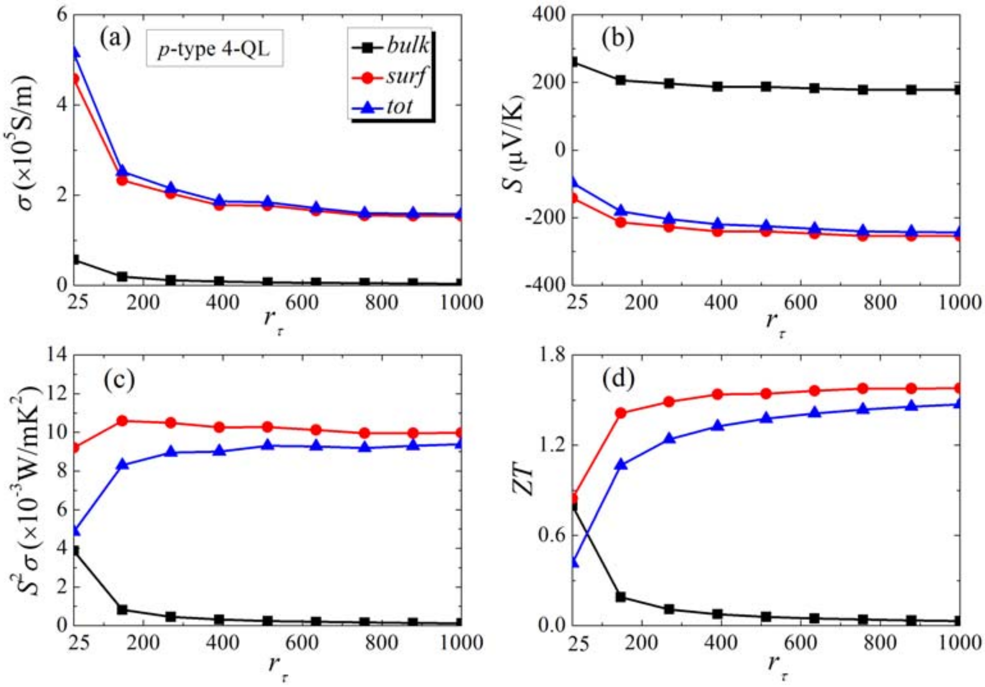

Figure S8 Calculated (a) electrical conductivity σ, (b) Seebeck coefficient S, (c) power factor $S^2\sigma$, and (d) figure of merit ZT of p-type 4-QL Bi_2Te_3 film as a function of the relaxation time ratio r_τ.

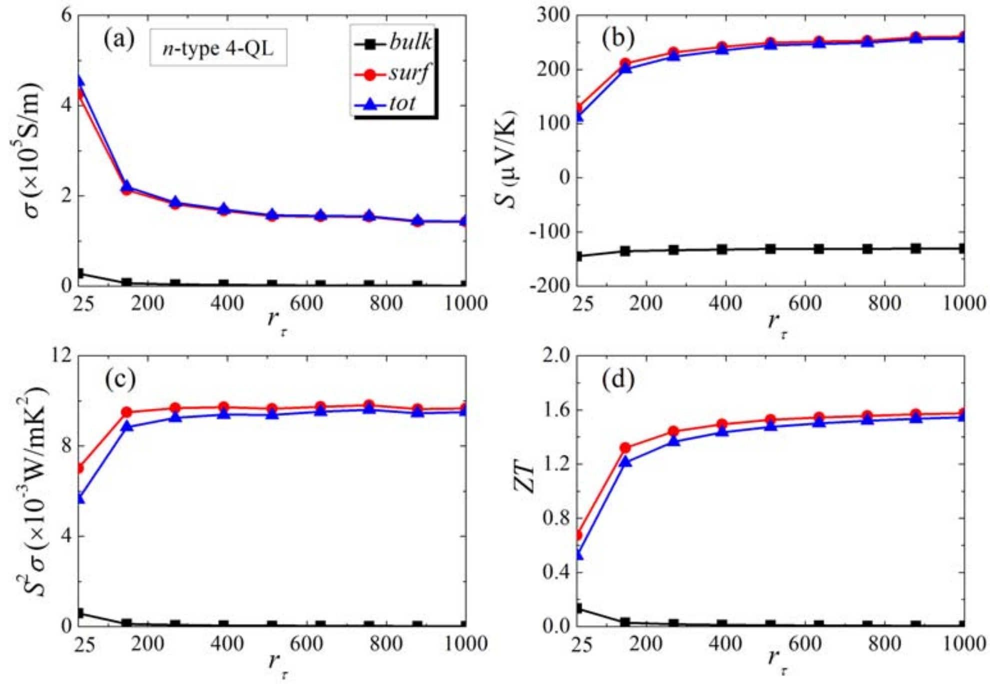

Figure S9 Calculated (a) electrical conductivity σ, (b) Seebeck coefficient S, (c) power factor $S^2\sigma$, and (d) figure of merit *ZT* of *n*-type 4-QL Bi_2Te_3 film as a function of the relaxation time ratio r_τ.

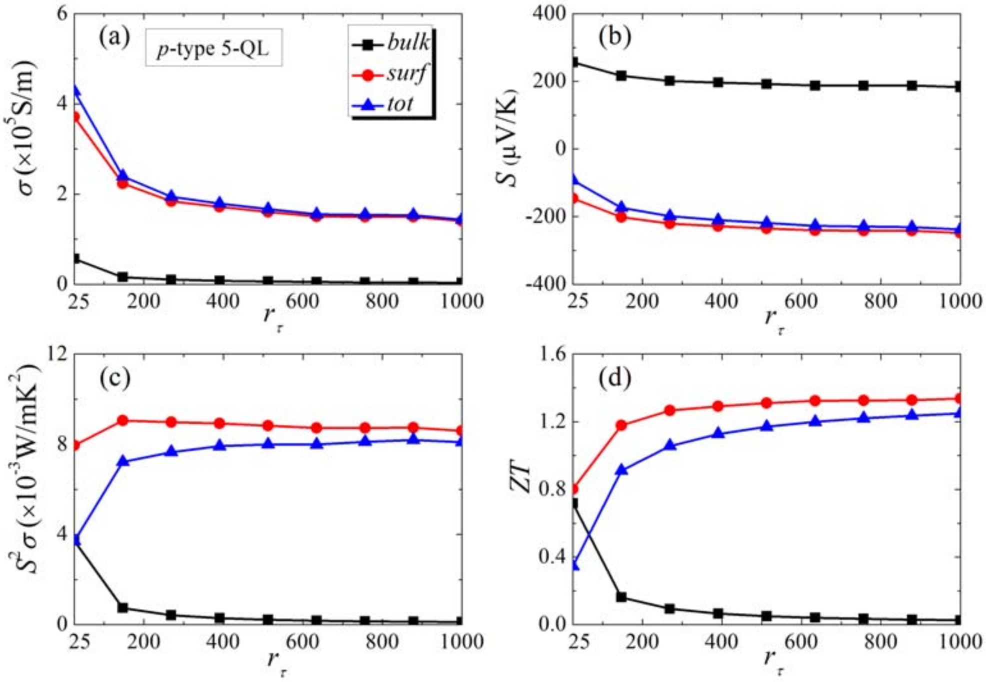

Figure S10 Calculated (a) electrical conductivity σ, (b) Seebeck coefficient S, (c) power factor $S^2\sigma$, and (d) figure of merit *ZT* of *p*-type 5-QL Bi_2Te_3 film as a function of the relaxation time ratio r_τ.

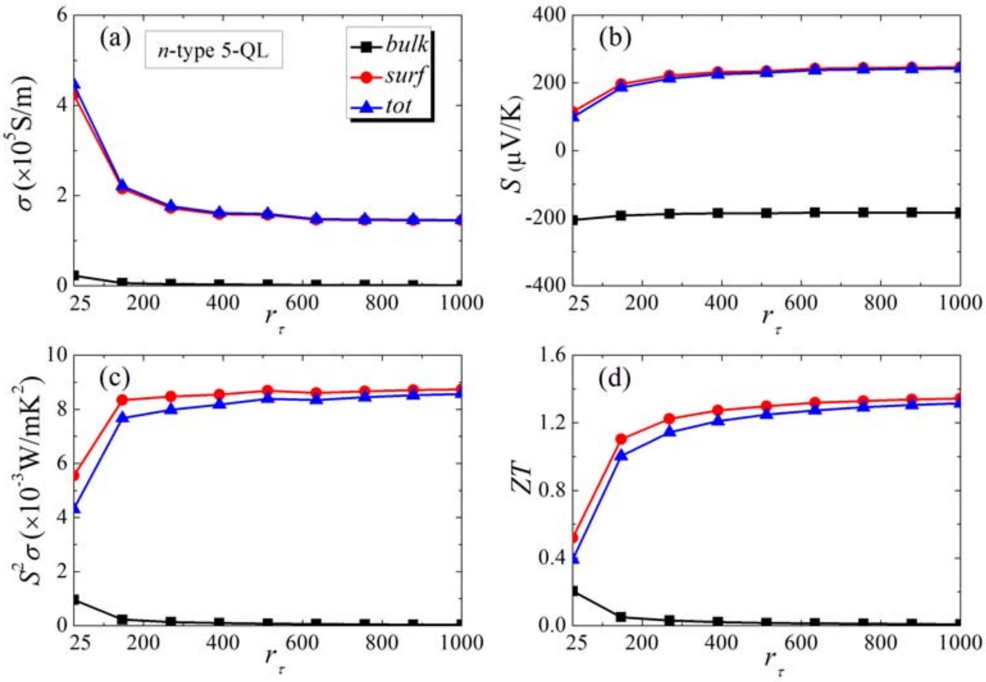

Figure S11 Calculated (a) electrical conductivity σ, (b) Seebeck coefficient S, (c) power factor $S^2\sigma$, and (d) figure of merit *ZT* of *n*-type 5-QL Bi_2Te_3 film as a function of the relaxation time ratio r_τ.

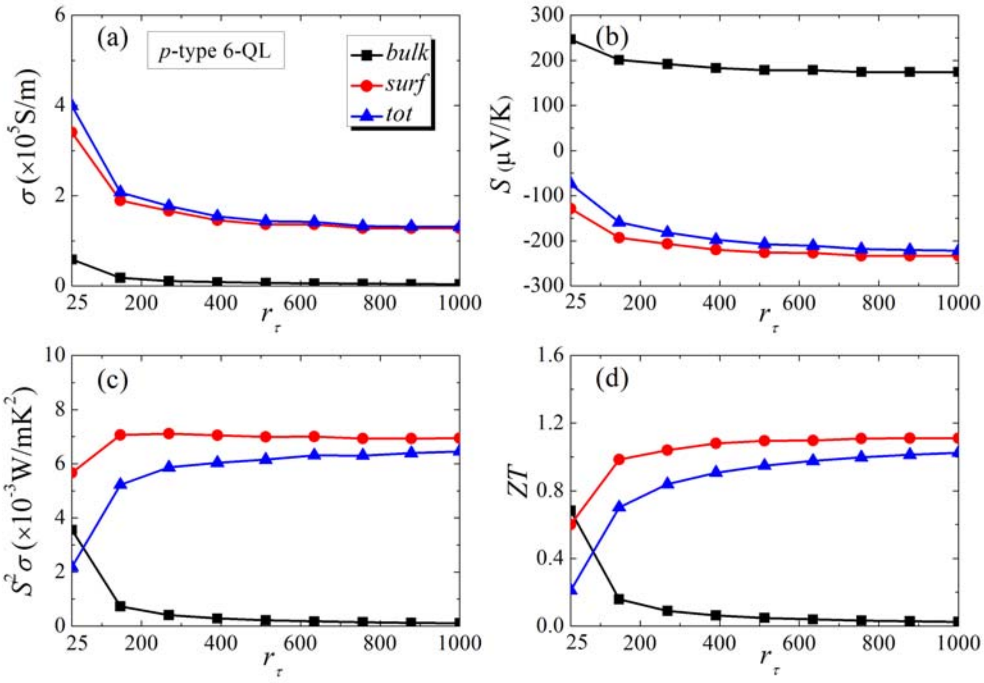

Figure S12 Calculated (a) electrical conductivity σ, (b) Seebeck coefficient S, (c) power factor $S^2\sigma$, and (d) figure of merit *ZT* of *p*-type 6-QL Bi_2Te_3 film as a function of the relaxation time ratio r_τ.

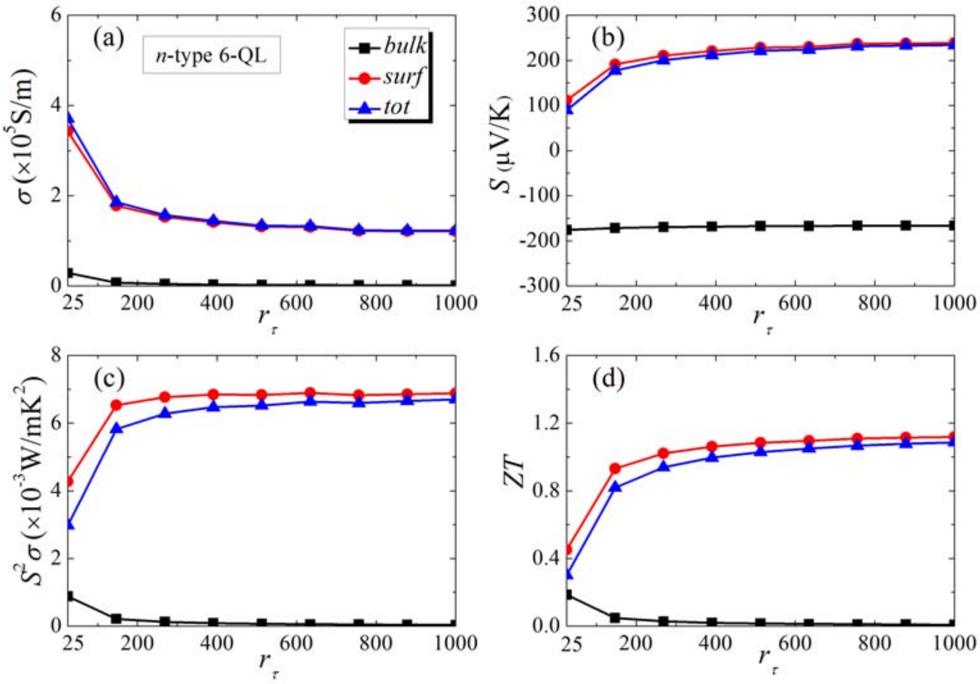

Figure S13 Calculated (a) electrical conductivity σ, (b) Seebeck coefficient S, (c) power factor $S^2\sigma$, and (d) figure of merit *ZT* of *n*-type 6-QL Bi_2Te_3 film as a function of the relaxation time ratio r_τ.

5. Thickness-dependent *ZT* values of Bi_2Te_3 films calculated by using different relaxation time ratio (Figure S14) or lattice thermal conductivity (Figure S15-S16). We can see that the non-monotonous behavior is very robust, which do not depend on the exact value of the relaxation time ratio or the variation of lattice thermal conductivity.

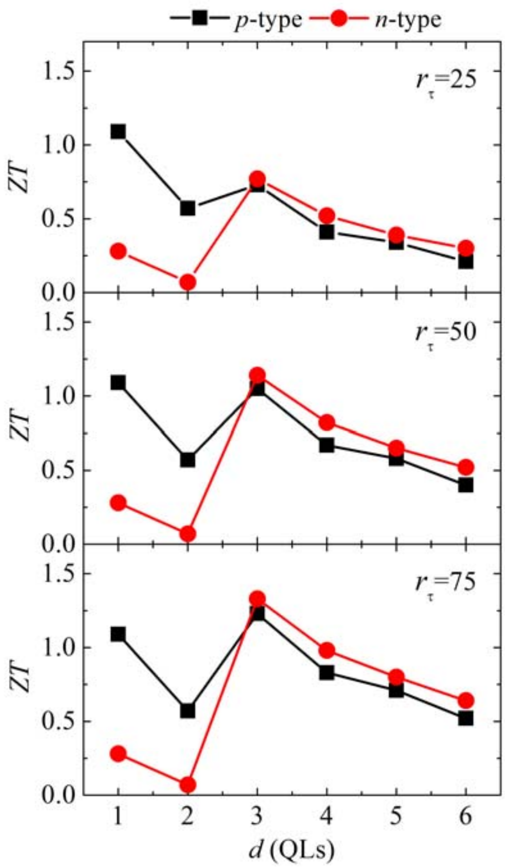

Figure S14 Thickness-dependent *ZT* values of Bi_2Te_3 films calculated by using three different relaxation time ratios, plotted as an addition to those shown in Figure 4.

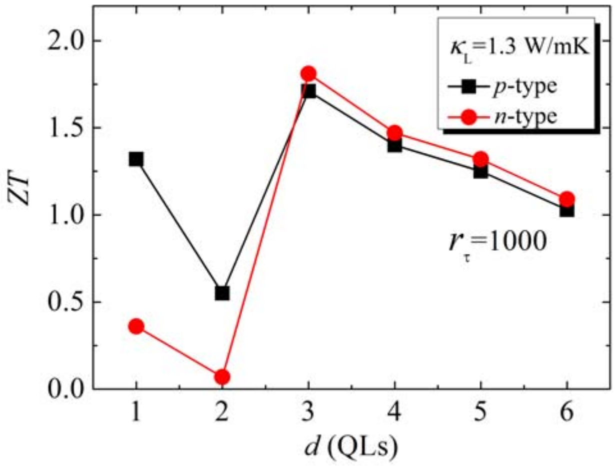

Figure S15 Thickness-dependent *ZT* values of Bi_2Te_3 films with relaxation time ratio of 1000, where an average lattice thermal conductivity of 1.3 W/mK is used for all the investigated QL systems.

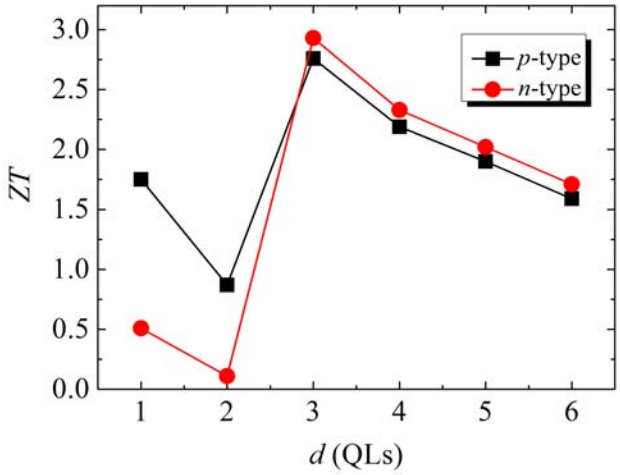

Figure S16 Thickness-dependent *ZT* values of Bi_2Te_3 films with relaxation time ratio of 1000, which is the same as that indicated in Figure 4(b) except that the lattice thermal conductivity of each QL system is assumed to be reduced by half.

6. The lattice thermal conductivity and the optimized carrier concentrations of Bi_2Te_3 films.

Table S1 The lattice thermal conductivity of Bi_2Te_3 films with thicknesses *d* = 1~6 QLs, which is obtained from Reference 37.

d (QLs)	1	2	3	4	5	6
κ_L (W/mK)	1.7	1.25	1.1	1.2	1.3	1.3

Table S2 The optimized carrier concentration n ($\times 10^{20}$ cm^{-3}) of *p*- and *n*-type Bi_2Te_3 films with thicknesses *d* = 3~6 QLs at three typical r_τ values of 25, 100, and 1000.

	3-QL		4-QL		5-QL		6-QL	
r_τ	*p*-type	*n*-type	*p*-type	*n*-type	*p*-type	*n*-type	*p*-type	*n*-type
25	0.18	0.57	0.02	0.52	0.01	0.45	0.01	0.37
100	0.37	0.66	0.16	0.58	0.08	0.53	0.09	0.43
1000	0.64	0.74	0.34	0.66	0.23	0.60	0.22	0.49